Mon. Not. R. Astron. Soc. **351,** 891–902 (2004) doi:10.1111/j.1365-2966.2004.07835.x

Dynamical friction for dark halo satellites: effects of tidal mass loss and growing host potential

HongSheng Zhao[1,2]★†

[1] *University of St Andrews, Physics and Astronomy, North Haugh, St Andrews, Fife KY16 9SS*
[2] *Institute of Astronomy, Madingley Road, Cambridge CB3 0HA*

Accepted 2004 March 9. Received 2004 March 8; in original form 2003 August 22

ABSTRACT

Motivated by observations of inner halo satellite remnants like the Sgr stream and ω Centauri, we develop fully analytical models to study the orbital decay and tidal mass loss of satellites on eccentric orbits in an isothermal potential of a host galaxy halo. The orbital decay rate is often severely overestimated if applying Chandrasekhar's formula without correcting for (i) the evaporation and tidal loss of the satellite, and (ii) the contraction of satellite orbits due to adiabatic growth of the host galaxy potential over the Hubble time. As a satellite migrates inwards, the increasing halo density affects the dynamical friction in two opposite ways: (1) it boosts the number of halo particles swept in the gravitational 'wake' of the satellite, hence increasing the drag on the satellite, and (2) it boosts the tide which 'peels off' the satellite, and reduces the amplitude of the wake. These competing processes can be modelled analytically for a satellite with the help of an empirical formula for the mass-loss history. The analytical model agrees with more traditional numerical simulations of tidal mass loss and dynamical friction. Rapid mass loss due to increasing tides at smaller and smaller radius makes it less likely for streams or remnants of infalling satellites to intrude into the inner halo (like the Sgr stream and ω Centauri) than to stay in the outer halo (like the Magellanic stream), hence any intermediate-mass central black holes of the satellites are also probably 'hung up' at large distances as well. It is difficult for the black holes of the satellites to come close enough to merge into the supermassive black hole in the centre of the host potential unless the satellites started with (i) pericentres much smaller than the typical distances to present-day observed satellites, and (ii) central density much higher than in the often seen finite-density cores of observed satellites.

Key words: methods: analytical – Galaxy: halo – Galaxy: kinematics and dynamics – galaxies: dwarf – dark matter.

1 INTRODUCTION

The current theory of galaxy formation favours the idea that galaxies form hierarchically by merging smaller lumps or satellites. The gravity from a moving satellite pulls behind it a 'wake' of particles of the host galaxy (Chandrasekhar 1943; Mulder 1983). This dynamical friction dissipates the orbital energy of the satellites so that they sink deep into the host galaxy potential well, where they are disintegrated and virialized via baryonic feedbacks and tidal stripping. These processes may have determined the density profile of virialized halo of the host galaxy (Syer & White 1998; Dekel, Devor & Hetzroni 2003).

There are about 150 and 300 globular clusters, and a few dozen dwarf satellites of mass 10^{6-9} $M_\odot$ in the Milky Way and M31 respectively. It is tempting to associate these dwarf satellites and globular clusters as the markers/remnants of past hierarchical merging events. Indeed, there are several examples of possible streams of remnants in the Milky Way (Lynden-Bell & Lynden-Bell 1995), including the recently found Galactic ring or Carnis Major dwarf galaxy, traced by a grouping of globular clusters (Martin et al. 2004). A giant stream is found in the Andromeda galaxy (Ferguson et al. 2002; McConnachie et al. 2003). Among these, the Sagittarius dwarf galaxy stream (Ibata et al. 1997) between radii 10 and 50 kpc from the Galactic Centre, is perhaps the best example. It brings in at least five globular clusters to the inner halo, including M54, the second most massive cluster of the Milky Way. A still mysterious object

★UK PPARC Advanced Fellowship and Visiting Professorship at Beijing Observatory.
†E-mail: hz4@st-andrews.ac.uk

is ω Centauri, with about 10^6 $L_\odot$ at 5 kpc from the Galactic Centre, which has the morphology of a globular cluster, but has multiple epochs of star formation and chemical enrichment [see Gnedin et al. (2002) and the ω Centauri symposium (van Leeuwen et al. 2002)]. Another example is the G1 cluster, a very massive globular-like object with about 10^6 $L_\odot$ at about 40 kpc from the M31 centre (Meylan et al. 2001). A system (NGC 1023-13) almost identical to G1 is also found in the S0 galaxy NGC 1023, at a projected distance of about 40 kpc from the host galaxy (Larsen 2001). Freeman (1993) suggested that such systems are the remnants of nucleated dwarf satellites, with their outer tenuous dark matter and stars being removed by galaxy tides. M31 also has an unusual collection of clusters as luminous as ω Centauri within 5 kpc in projection from its double-peaked centre. Given the above evidence or signs of infalling objects in our Galaxy and M31, it is interesting to ask whether some of the inner globulars could have also been the result of mergers. Beyond the Local Group, minor mergers are sometimes speculated as the mechanism by which to deliver massive black holes and gas material into the nucleus of an active galaxy to account for the directions of the jets and nuclear dusty discs (Kendall, Magorrian & Pringle 2003). A very interesting related issue is whether giant black holes acquire part of their mass by merging the smaller black holes in the nuclei of infalling satellites.

For this paper we revisit the basic theoretical questions: what is the condition for a dwarf galaxy to decay into the inner halo? What are the possible outcomes of tidal stripping of a dwarf satellite? How often do we get a system like ω Centauri or a naked black hole near the host centre? The answers to these questions will help us to test the validity of the theory of hierarchical merger formation of galaxies. The key mechanism for satellites to enter the inner galaxy is dynamical friction, where the gravity of the satellite creates a wake of overdensities in the particle distribution of the host galaxy, which in turn drags the motion of the satellite with a force proportional to $m(t)^2$, where $m(t)$ is the mass of the satellite. Another process is tidal disruption, where the object sheds mass with each pericentre passage, and the remnants are littered along the orbit of the satellite. The above two processes compete with and regulate each other: orbital decay increases the tidal field, which reduces the mass of the satellite, and hence slows down the orbital decay. Some examples of these effects have been shown by Zhao (2002) in the case of ω Centauri.

The analytical formula of Chandrasekhar is widely used for gaining insights on dynamical friction because of the time-consuming nature of the more rigorous N-body numerical simulation approach. It is a customary practice in previous works to model the orbital decay of a satellite as a point mass of a fixed mass. However, *the fixed-mass approximation is invalid* and could seriously overestimate dynamical friction because of the neglect of mass loss $\mathrm{d}m(t)/\mathrm{d}t$. It is essential in calculations of satellite orbits to model the dynamical friction and mass loss together since they regulate each other.

In the past the mass loss and the orbital decay have often been modelled in an *ab initio* fashion, resulting in coupled non-linear equations without simple analytical solutions. In such models, the satellite mass is often modelled as a function of the tidal radius of the satellite, hence various factors come in, including the orbital position of the satellite and the density profile of the satellite (e.g. Jiang & Binney 2000; Zhao 2002; Mouri & Taniguchi 2003; Kendall et al. 2003). However, these complications are not always necessary since the mass-loss history is rather similar in simulations with very different initial conditions (the mass is generally a staircase-like function of the time), so could be parametrized in an empirical fashion, bypassing the uncertain assumptions of the satellite initial profile. This could be useful for exploring a large parameter space of the satellite initial conditions.

Another invalid approximation but common practice is to use a static potential for the host galaxy. This again is unphysical since galaxy haloes do grow in the hierarchical formation scenario partly because of galaxy merging, and partly because of the adiabatic contraction of the baryonic disc and bulge; galaxy rotation curves $V_{\rm cir}(r, t)$ can change significantly before and after the formation of baryonic discs and bulges in mass models for the Milky Way and M31 (Klypin, Zhao & Somerville 2002) and in generic cold dark matter simulations with baryons (e.g. Wright 2003). The growing gravitational force tends to restrain the radial excursions of the satellite while preserving the angular momentum. The dynamical friction or drag force is also proportional to the growing density $\rho(r, t)$ of ambient stars and dark particles in the host galaxy.

In fact, it is conceptually simple to incorporate mass loss and growing potential while keeping the problem analytically tractable: the deceleration $-\mathrm{d}v/\mathrm{d}t$ is simply proportional to the satellite mass $m(t)$ and the ambient density $\rho(r, t)$ of the host galaxy at the time t. Without mass loss Chandrasekhar's formula would predict very efficient braking of the orbits, enough to make a high-mass satellite of $\sim 10^{10}$ $M_\odot$ (the mass of the Large Magellanic Cloud (LMC) or a M33-sized object) decay from a circular orbit at $\sim$100 kpc to the very centre of a high-brightness galaxy in a Hubble time, delivering remnants into the inner galaxy. Here we study the effect of mass loss and growing potential on the result of orbital decay, and the distribution of remnants. We present fully analytical results for calculating the decay rate for satellites on eccentric orbits in a scale-free growing isothermal potential.

The structure of the paper is as follows: Section 2 gives the analytical formulation of the problem, Section 3 presents results of application to globulars and dwarf satellites, Section 4 studies the relation between mass loss and the satellite density profile. Section 5 discusses the progenitors of Sgr and ω Centauri, and Section 6 summarizes.

2 ANALYTICAL ORBITAL DECAY MODEL FOR A SHRINKING SATELLITE IN A GROWING HOST

Consider a satellite moving with a velocity $\boldsymbol{v}_{\rm s}$ on a rosette-like orbit in a spherical host galaxy potential $\phi(r, t)$ with a rotation curve $V_{\rm cir}$. Assume that it has an initial mass $m_{\rm i}$; the orbital decay from an initial time $t = t_{\rm i}$ to the present day $t = t_0$ can be modelled using Chandrasekhar's dynamical friction formula (Binney & Tremaine 1987)

$$\frac{\mathrm{d}\boldsymbol{v}_{\rm s}}{\mathrm{d}t} = -\frac{\boldsymbol{v}_{\rm s}}{t_{\rm frc}} - \frac{V_{\rm cir}^2}{r^2}\boldsymbol{r}, \tag{1}$$

where $t_{\rm frc}$ is the instantaneous dynamical friction time. Manipulating the equation, we find that the (specific) angular momentum $j(t)$ of the satellite decays as

$$\frac{\mathrm{d}\boldsymbol{j}(t)}{\mathrm{d}t} = \boldsymbol{r}\times\frac{\mathrm{d}\boldsymbol{v}_{\rm s}}{\mathrm{d}t} = -\frac{\boldsymbol{j}(t)}{t_{\rm frc}}, \qquad \boldsymbol{j}(t) = \boldsymbol{r}(t)\times\boldsymbol{v}_{\rm s}(t). \tag{2}$$

Here the dynamical friction time is given by

$$t_{\rm frc}^{-1} = [4\pi G\rho(r, t)]\,\frac{Gm(t)}{V_{\rm cir}^3}\xi(u), \qquad u(t) \equiv \left(\frac{|\boldsymbol{v}_{\rm s}|}{V_{\rm cir}}\right), \tag{3}$$

where $m(t)$ is the mass of the satellite, $\rho(r,t)$ is the density of the host galaxy at the orbital radius $r(t)$, and the effect of the satellite speed $|\,\boldsymbol{v}_{\rm s}|$ is contained in $\xi(u)$, which is some dimensionless function of the rescaled satellite speed u.

Here we adopt a singular isothermal spherical (SIS) host galaxy model with a rotation curve generally growing with time $V_{\rm cir}(t)$; it is normalized by the present-time value $V_{\rm cir}(t_0)=V_0$. In this model the potential and density are given by

$$\phi(r,t)=V_{\rm cir}^2(t)\ln r, \qquad \rho(r,t)=\frac{V_{\rm cir}^2(t)}{4\pi G r^2}. \tag{4}$$

Since the velocity distribution of stars and dark matter in the host galaxy is an isotropic Gaussian, the dimensionless velocity function

$$\xi(u)=u^{-3}\left[{\rm erf}(u)-\frac{2u}{\sqrt{\pi}}\exp(-u^2)\right]\ln\Lambda \approx \frac{\ln\Lambda}{\frac{4}{3}+u^3}, \tag{5}$$

where the dimensionless Coulomb logarithm $\ln\,\Lambda$ is typically between unity and 10. It is easy to verify that our *simple approximation* for $\xi(u)$ works to 10 per cent accuracy for $0\leqslant u=(|\boldsymbol{v}_{\rm s}|/V_{\rm cir})<\infty$, which is accurate enough in practice because real velocity distributions are often slightly non-Gaussian anyway. Note that for very low speed $\xi(0)/\ln\Lambda = 4/3\sqrt{\pi}\approx 3/4$ and for circular motion $\xi(1)/\ln\Lambda={\rm erf}(1)-(2/e\sqrt{\pi})\approx 3/7$.

Combining the above equations, we find that the decay rate for (the amplitude of) the angular momentum is given by[1]

$$\frac{{\rm d}j(t)}{{\rm d}t}=-\frac{j(t)}{t_{\rm frc}}, \qquad \frac{1}{t_{\rm frc}}=\frac{G\mu(t)V_{\rm cir}(t)}{j(t)^2}, \tag{6}$$

where we define an effective bound mass of the satellite at time t

$$\mu(t)\equiv m(t)\beta(t), \qquad \beta(t)=\xi(u)u^2\cos^2(\alpha), \tag{7}$$

where $u(t)=|\,\boldsymbol{v}_{\rm s}(t)|/V_{\rm cir}(t)$ and $\alpha(t)$ are the rescaled speed and the pitch angle of the orbit at time t. As we can see, the effective mass $\mu(t)$ lumps together several time-varying factors. It is proportional to the satellite mass $m(t)$ by a dimensionless factor $\beta(t)$ which incorporates the varying efficiencies of dynamical friction in an orbital epicycle. Note that $\beta(t)$ is an oscillating function of time of order unity, which we will come to in Section 2.2. Introducing this *effective* mass simplifies the details of the physics because the braking rate of specific angular momentum $-{\rm d}j(t)/{\rm d}t$ is now simply proportional to $\mu(t)$.

Integrating over time, we find that the change in the specific angular momentum between time $t_{\rm i}$ and t_0 is given by

$$-\Delta j^2=j^2(t_{\rm i})-j^2(t_0)=2G\mu_{\rm i}V_0\tau,$$
$$\tau\equiv(t_{\rm i}-t_0)\gamma\equiv\int_{t_{\rm i}}^{t_0}\frac{\mu(t)V_{\rm cir}(t)}{\mu_{\rm i}V_0}{\rm d}t, \tag{8}$$

where we define γ as the reduction factor from the fixed-mass satellite model, and define τ as the effective duration of dynamical friction; $\mu_{\rm i}$ and V_0 are the effective mass at initial time $t_{\rm i}$ and the rotation curve at the present t_0. The above formula allows us to calculate the evolution of the specific angular momentum $j(t)$ of a generally *eccentric satellite orbit*.

It is interesting to ask what the necessary condition is for an outer halo satellite to reach the inner galaxy or even the centre. These satellites will be destroyed with their remnants in the inner galaxy, e.g. by the disc and/or bulge shocking. To facilitate the comparison with observations, it is sometimes better to define an instantaneous orbital size[2]

$$S(t)\equiv\frac{j(t)}{V_0} \tag{9}$$

at time t. Let the present orbital size $S_0=j_0/V_0\leqslant R_{\rm disc}\sim 15$ kpc, and define $j_{\rm disc}=R_{\rm disc}\times V_0$ as the critical angular momentum to reach within the disc at the present time. Manipulating equation (8), we find that the initial angular momentum $j_{\rm i}$ or orbital distance $S_{\rm i}=j_{\rm i}/V_0$ must satisfy

$$S_{\rm i}=\left(S_0^2+\frac{2G\mu_{\rm i}\tau}{V_0}\right)^{1/2}, \qquad 0\leqslant S_0\leqslant R_{\rm disc}, \tag{10}$$

where τ is given in equation (8). In other words, satellites initially on orbits larger than $S_{\rm i}$ would not be able to deliver a globular or dwarf galaxy to the inner galaxy irrespective of mass loss assumed.

2.1 A geometrical interpretation

Equation (8) is our main analytical result. There is also an interesting geometrical interpretation to it. Consider, for example, a satellite of mass $m(t)$ on a *circular orbit* in a static SIS potential; we have

$$\begin{aligned}&\ln\Lambda\approx 2.5,\\ &\beta(t)=\xi(1)\times 1^2=0.42\ln\Lambda\approx 1,\\ &\mu(t)=m(t)\beta(t)\approx m(t),\end{aligned} \tag{11}$$

where we have taken a typical value for the Coulomb logarithm (e.g. Penarrubia, Kroupa & Boily 2002). We can rewrite the angular momentum equation (equation 8) as

$$\left|\pi\Delta S^2\right|\approx\frac{2\pi G\langle m\rangle}{V_0^2}\left(V_0\Delta t\right), \qquad \langle m\rangle=\frac{\int_{t_{\rm i}}^{t_0}m(t){\rm d}t}{t_0-t_{\rm i}}, \tag{12}$$

where the left-hand side is the area swept by the decaying orbit, and on the right-hand side $2\pi\,G\,\langle m\rangle\,V_0^{-2}$ is the 'circumference of influence' of the satellite and $V_0\Delta t=V_0(t_0-t_{\rm i})$ is the length of the orbital path of the satellite, and the multiplication of the two is the area swept by the circumference of influence of the satellite. The above equation implies that the two areas are comparable. Interestingly, the decay of the orbits depends on the satellite mass through the approximation $\Delta S^2\propto\langle m\rangle\,\Delta t$, i.e. it is the average mass of the satellite that determines the rate of orbital decay. Finally, note that equation (8) applies to the evolution of specific angular momentum of an eccentric orbit in a time-varying potential. A complete description of the orbits should also include the evolution of the orbital energy, which unfortunately is more complex analytically, and is not studied in detail here. It is not essential for our conclusion, but is perhaps convenient to assume efficient dynamical decay of the orbital energy during the pericentric passages; hence the radial motion is damped and the orbit circularizes at the end. Adiabatic growth of the potential also tends to circularize the orbits.

2.2 Modelling the growing host potential

The classical singular isothermal model assumes a fixed potential or a time-invariant rotation curve. In reality galaxies grow substantially

[1] The dynamical friction time $t_{\rm frc}$ is now expressed in terms of the angular momentum $j(t)$ instead of $r(t)$ with the help of substitutions $r(t)\rightarrow j(t)/[|\boldsymbol{v}_{\rm s}(t)|\cos\alpha(t)]$ and $|\boldsymbol{v}_{\rm s}(t)|\rightarrow u(t)\,V_{\rm cir}$.

[2] We can make this definition irrespective of the eccentricity of the orbit, which does not enter our calculation explicitly. Roughly speaking, the orbital size $S(t)$ is the geometrical mean of the pericentre radius and apocentre radius in a static potential.

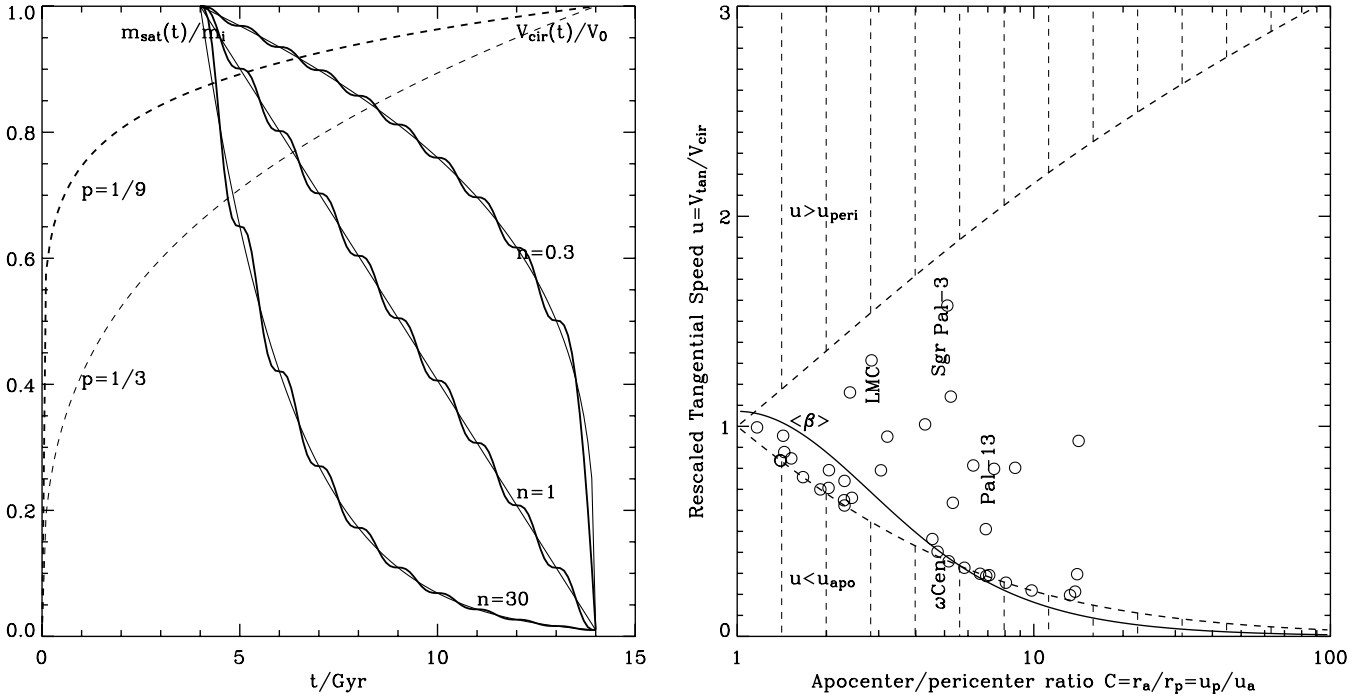

Figure 1. Panel (a) (left) shows the rescaled satellite mass $m(t)/m_{\rm i}$ (thick solid line) and effective mass $\mu(t)/\mu_{\rm i}$ (thin solid line) as a function of time for three models (marked by their n-values), and the rescaled host halo rotation speed $V_{\rm cir}(t)/V_0$ for the past Hubble time for two models (marked by their p-values). Panel (b) (right) shows the boundaries of the rescaled tangential speed $V_{\rm a}/V_{\rm cir} \leqslant u \leqslant V_{\rm p}/V_{\rm cir}$, (lower and upper dashed lines) as functions of the apocentre-to-pericentre ratio $C = r_{\rm a}/r_{\rm p} = V_{\rm p}/\,V_{\rm a}$. Also shown is the mean effective mass conversion factor $\langle\beta\rangle = \mu/m$ (solid line, cf. equation 21), normalized to $\ln\Lambda = 2.5$. Note that the value of $\langle\beta\rangle$ varies by *only* a factor of 2 among the Milky Way satellites and globular clusters (circles); the pile-up of some clusters along the apocentre line is due to distance errors [data taken from Dinescu et al. (1999) and references therein].

from redshifts of a few to now. The growth of the dark halo is scale-free in the hierarchical scenario, so it is plausible to approximate the growth of the rotation curve as a power law in time as follows:

$$V_{\rm cir}(t) = V_0 \left(\frac{t}{t_0}\right)^p, \qquad 0 < t < t_0, \tag{13}$$

where the rotation speed at some earlier time $0 < t < t_0$ is generally smaller than the present-day ($t = t_0 = 14$ Gyr) value V_0. At the present epoch $V_{\rm cir}(t_0) = V_0 = 200$ km s^{-1} is appropriate for the Milky Way. A few sample evolution models are shown in Fig. 1(a). A value of $1/9 \leqslant p \leqslant 1/3$ implies an evolution of 10–25 per cent in rotation speed from redshift 1 to now, which seems reasonable in models of the Milky Way before and after the formation of the disc and the bulge (Klypin et al. 2002; Wright 2003).

2.3 Modelling the shrinking satellite

Previously the tidal stripping of the satellite has been modelled either by N-body simulations (e.g. Johnston et al. 1999; Tsuchiya, Dinescu & Korchagin 2003) or semi-analytically using tidal radius criteria (e.g. Zhao 2002; Kendall et al. 2003).[3] In both approaches one needs to assume a rigorous description of the mass profile of the progenitor satellite. It is unclear whether this approach can model efficiently the realistic large scatter in the circular velocity curves of observed dwarf galaxies.

[3] Recently the latter approach has also been extended to model the orbital decay and evaporation-induced mass loss in the dense star cluster near the Galactic Centre (Mouri & Taniguchi 2003; McMillan & Portegies-Zwart 2003).

Here we take a very different approach. We model the mass of the progenitor galaxy as a simple function of time with two free parameters. We do not need an explicit prescription of the satellite density profile. Motivated by the mass-loss history typically seen in N-body simulations, the satellite mass is modelled to decay at a rate between exponential and linear mass loss. To simplify the calculations, we lump together several uncertain factors, and simply assume that the *effective* mass of the satellite is shed following the following recipe:

$$\begin{aligned}
\mu(t) &= \langle\beta\rangle_{\rm i} m_{\rm i} \left\{1 - \left[1 - \left(\frac{\langle\beta\rangle_0 m_0}{\langle\beta\rangle_{\rm i} m_{\rm i}}\right)^{1/n}\right]\hat{t}\right\}^n, \\
\hat{t} &= \frac{t - t_{\rm i}}{t_0 - t_{\rm i}}, \\
m(t) &= m_{\rm i}\left\{1 - \left[1 - \left(\frac{m_0}{m_{\rm i}}\right)^{1/n}\right]\hat{t}_N\right\}^n, \\
\hat{t}_N &= \hat{t} - \frac{\sin 2N\pi\hat{t}}{2N\pi} \approx \hat{t},
\end{aligned} \tag{14}$$

where m_0 and $m_{\rm i}$ are the mass at the present $t = t_0 = 14$ Gyr and when the satellite falls in at $t = t_{\rm i}$, $0 \leqslant \hat{t} \leqslant 1$ is the rescaled dimensionless time, and $N \sim 1$–100 is the total number of pericentric passages between time t_0 and $t_{\rm i}$. The parameters $\langle\beta\rangle_{\rm i}$ and $\langle\beta\rangle_0$ are the initial and final effective mass conversion factors, which we will come to.

The parameter n determines the profile of the mass-loss history. It is tunable, with the $n = 1$ model having a constant rate of mass loss, and the $n \to \infty$ having an exponential mass loss; and $n = -1$ is a roughly power-law decay. In simulations we typically see somewhere in between these cases: $0 < n \leqslant 1$ for Plummer or King model satellites with a sharp fall-off after an initially linear mass

loss (e.g. Penarrubia et al. 2002); for isothermal satellite models, the mass loss is close to linear $n = 1$ (Zhao 2002). Note that for a completely disrupted satellite $m_i \gg m_0 \sim 0$. In N-body simulations, the satellite loses mass mainly in bursts near pericentric passages, so the mass is a descending staircase-like function of time. This is simulated fairly well by our formula with $\hat{t}_N$ in $m(t)$: a few examples of mass-loss histories are shown in Fig. 1(a) where we assume $N = 10$ pericentric passages from $t_i = 4$ Gyr to now $t_0 = 14$ Gyr.

2.4 Modelling the effective mass conversion factor $\langle\beta\rangle$

The conversion factor between the effective mass $\mu(t)$ and the actual mass $m(t)$ of the satellite is given by

$$\beta(t) = \frac{\mu(t)}{m(t)} = \xi(u)\,(u\cos\alpha)^2\,, \tag{15}$$

where u is the rescaled satellite velocity at time t and $\alpha(t)$ is the pitch angle. To compute the average value of $\beta(t)$ over one epicycle, let us first define C as the ratio of the apocentre r_a to pericentre r_p, or the ratio of pericentre velocity $u_a V_{cir}$ and $u_p V_{cir}$, where

$$u_p V_{cir} = \frac{j}{r_p}, \qquad C \equiv \frac{r_a}{r_p} = \frac{u_p}{u_a}. \tag{16}$$

According to energy conservation we have

$$\frac{E}{V_{cir}^2} = \frac{u_p^2}{2} + \ln r_p = \frac{u_a^2}{2} + \ln r_a, \tag{17}$$

where E is the energy at pericentre and apocentre. It is easy to show that r_p and u_p are determined by the angular momentum j and the circular velocity V_{cir} as follows:

$$r_p = j V_{cir}^{-1} u_p^{-1}, \qquad u_p = \sqrt{\frac{2\ln C}{1 - C^{-2}}}. \tag{18}$$

Now if we make the approximations that

$$\frac{\mu(t)}{m(t)} \approx \langle\beta(t)\rangle \approx \xi(\langle u\rangle)\langle u^2\cos^2\alpha\rangle \tag{19}$$

and the further approximations

$$\langle u^2\cos\alpha^2\rangle \approx u_p u_a, \qquad \langle u\rangle \approx \left(\frac{u_p^{2k} + u_a^{2k}}{2}\right), \qquad k = \frac{9}{11}, \tag{20}$$

then we have

$$\begin{aligned} \frac{\mu(t)}{m(t)} &\approx \langle\beta(t)\rangle \approx \xi\left(\langle u\rangle\right)\left(\frac{2\ln C}{C - C^{-1}}\right), \\ \langle u\rangle \quad &= \frac{C^k + C^{-k}}{2}\left(\frac{2\ln C}{C - C^{-1}}\right)^k, \qquad k = \frac{9}{11}. \end{aligned} \tag{21}$$

Equation (21) is then checked with the time averages computed by direct numerical integration of the orbit from pericentre to apocentre, and is found to be accurate to 2 per cent for $1 \leqslant C \leqslant 100$ (a simpler expression with $k = 1$ gives somewhat poorer accuracy). While we neglect variation of β within one epicycle, there can still be secular evolution because the orbital energy is lost more efficiently at pericentre, hence the orbit tends to circularize, which increases the effective mass conversion factor $\langle\beta\rangle$. Generally speaking, the factors $\langle\beta\rangle$, u_p and u_a etc. are functions of C, which can be read from the curves in Fig. 1(b). For those Milky Way satellites and globular clusters for which we have good proper motions, the C-values are typically between 1 and 10 (Dinescu, Girard & van Altena 1999), hence $\langle\beta\rangle$ varies only by a factor of at most 3 for these satellites. So the uncertainty of their effective masses $\mu = \langle\beta\rangle\, m$ is still largely from errors of their observed mass-to-light ratios.

The above conversion factor should be a good approximation for eccentric satellite orbits with apocentre-to-pericentre ratio of C in a flat rotation curve potential. For example, for an apocentre-to-pericentre ratio $C = r_a/r_p = 5$, we have a rescaled pericentre speed $u_p \approx \sqrt{3}$, and an average mass conversion factor $\langle\beta\rangle \approx 0.5 \times (0.42 \ln \Lambda)$. Assuming $\ln \Lambda = 2.5$, we have $\mu(t) \approx 0.5 m(t)$. In comparison $\mu(t) \approx m(t)$ for circular orbits. So for the same angular momentum, our model suggests that eccentric orbits have a smaller effective mass of the satellite, hence slower evolution of the orbital angular momentum.[4] It is interesting that all three factors, mass loss, growing potential and orbital eccentricity, all work in the same sense of reducing the evolution of orbital angular momentum.

For a rough estimation of the reduction of dynamical friction due to satellite mass loss and host growth, let us consider a *Gedanken* experiment where a satellite enters a growing host galaxy at time $t_i = 0$ right after the big bang and is completely dissolved ($\mu_0 = 0$) by the time t_0. Neglecting the sinusoidal component by letting $N \to \infty$, the reduction factor γ is computed by substituting equations (13)–(14) into equation (8). We find $\gamma = p!n!/(p + n + 1)! = 1/6$ if the satellite loses mass linearly with time ($n = 1$) in a linearly growing halo ($p = 1$). This estimate is perhaps to the extreme. In reality the formation and mergers of the satellites probably occur over an extended period of the Hubble time, perhaps starting around a redshift of 1.5 ($t_i = 4$ Gyr), ending around now ($t_0 = 14$ Gyr). Hereafter we consider mostly models with $t_i = 4$ Gyr, and $t_0 = 14$ Gyr, $0 \leqslant p \leqslant 1/3$ and $\mu_0 \ll \mu_i$.

3 RESULTS OF APPLICATION TO GLOBULARS AND DWARF SATELLITES

Section 2 gives the formalism to predict analytically the evolution of the angular momentum of the satellite for a satellite with any mass-loss history on an eccentric orbit around a time-varying potential.

Clearly not all satellites could reach the galactic centre as a globular or a naked massive black hole. Dynamical friction is basically turned off if the satellite bound mass drops below 10^9 $M_\odot$ before reaching the inner galaxy. To reach the inner, say, 15 kpc of the host galaxy, which is roughly the truncation radius of the outer disc of the Milky Way, a satellite must have presently a specific angular momentum

$$0 \leqslant j_0 \leqslant j_{disc} \equiv R_{disc} V_0 = 15\,\mathrm{kpc} \times 200\,\mathrm{km\,s^{-1}}. \tag{22}$$

In comparison, the present specific angular momenta of some of the known satellites are given in Table 1. The Magellanic stream and Ursa Minor have $j_0 \sim 15\,000$ km s^{-1} kpc, much larger than j_{disc}.

Suppose that there was a population of hypothetical dwarf satellites in the outer halo with a specific angular momentum comparable to that of the orbits of the LMC, Ursa Minor and Fornax. Suppose that their initial mass m_i is between those of Ursa Minor and the LMC (10^{7-10} $M_\odot$) at some time t_i between 4 and 14 Gyr. We integrate forward in time to answer the question of where their remnants are. Clearly the effect of orbital decay is maximized if we take the longest evolution time (10 Gyr), the highest initial satellite mass and the smallest initial orbit $j_i = 60$ kpc $\times$ 250 km s^{-1}. This is the case shown by the hatched region in Fig. 2 with the satellite starting from the upper right corner and ending to the lower left with a mass of 10^7 $M_\odot$. The vertical axis $S(t) = j(t)/200$ is a characteristic orbital distance of the satellite, expressed in terms of the specific angular

[4] However, the circularization of the orbit tends to enhance dynamical friction.

Table 1. Orbital size of known satellites of the Local Group.

Object	Spec. ang. mom. $j_0 = \boldsymbol{r}$ kpc $\times$ $\boldsymbol{v}$ km s^{-1}	Orbital size $S_0 \equiv j_0/200$ kpc	Ref.
ω Centauri	5 kpc $\times$ 50 km s^{-1}	1.25	(1)
Sgr stream	16 kpc $\times$ 260 km s^{-1}	20.8	(2)
Magellanic stream	60 kpc $\times$ 250 km s^{-1}	75	(3)
Ursa Minor	70 kpc $\times$ 200 km s^{-1}	70	(4)
Fornax	138 kpc $\times$ 310 km s^{-1}	213	(5)
M31 stream	150 kpc $\times$ 20 km s^{-1}	15	(6)
Canis Major dSph	15 kpc $\times$ 200 km s^{-1}	15	(7)

References: (1) Dinescu et al. (1999); (2) Ibata et al. (1997); (3) Kroupa & Bastian (1997); (4) Schweizer, Cudworth & Majewski (1997); (5) Piatek et al. (2002); (6) McConnachie et al. (2003); (7) Martin et al. (2004).

momentum divided by a characteristic velocity of 200 km s^{-1}. This orbital distance is roughly the geometrical mean of the apocentre and pericentre. Models are shown in order of increasing dynamical braking. The upper shaded zone shows models with between exponential and linear mass loss and a moderate evolution of the potential ($\infty \geqslant n \geqslant 1$, $p = 1/3$); the lower shaded zone shows models with between linear and accelerated mass loss and a static potential ($1 > n > 0.3$, $p = 0$). Qualitatively speaking, the orbital decay appears to be only modest in all cases; the remnants are generally not delivered to the inner galaxy.

The condition for a satellite to deliver a low-mass substructure to the inner halo (cf. equation 15) or a 10^6-M$_\odot$ black hole to the galaxy centre is summarized in Fig. 3. The satellite must be within 20 kpc for the past Hubble time for a low-mass (10^{7-9} M$_\odot$) progenitor. It could be at a modest distance of 40–50 kpc if the progenitor was very massive (10^{10} M$_\odot$) with a linear or accelerated mass loss ($n < 1$) and little evolution of the galactic potential ($\ll 1$). Progenitors of the inner halo substructures or central black hole cannot be on orbits of specific angular momentum comparable to those of the LMC, Ursa Minor or Fornax. This illustrates the difficulty of making systems such as ω Centauri as the nucleus of a stripped-off dwarf galaxy starting from the very outer halo. Likewise, it is difficult for a minor merger to bring in a million solar mass black hole to the host galaxy centre. The orbit of the progenitor must be radial and well-aimed at the galaxy centre such that the tangential velocity of the progenitor is $\leqslant 1$ km s^{-1} if the satellite comes from an initial distance of 1 Mpc.

4 COMPARISON OF VARIOUS MODELS FOR TIDES AND SATELLITE DENSITY PROFILES

The basic feature of our dynamical friction models is that they bypass any information on the satellite internal density profile and the varying tidal force on the satellite by specifying the effective mass $\mu(t)$ as an explicit empirical function of time directly. This immediately brings up several questions, which we answer in the next two subsections. (1) Is our analytical model accurate enough? Compared with a simulation with the more traditional 'tidal peeling' approach, does our model reproduce the overall rate of orbital decay for the same initial conditions? (2) Can our analytical model be used to infer the underlying mass profile for satellites? Is the inferred mass profile plausible for observed satellites?

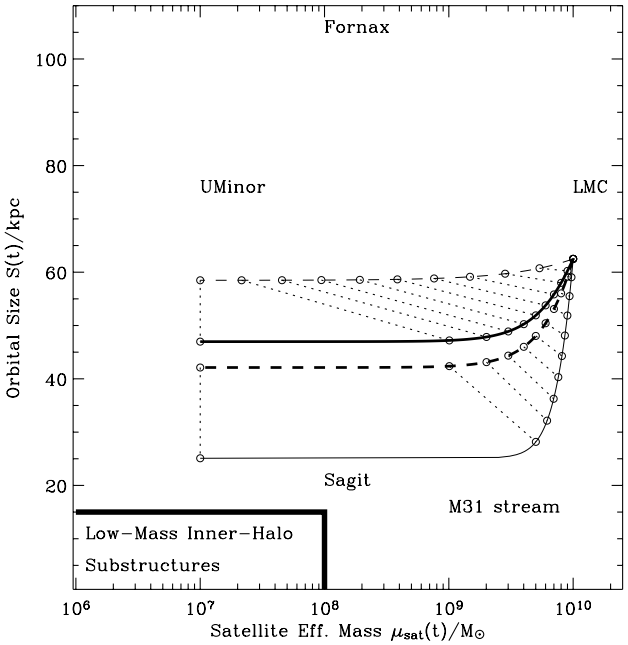

Figure 2. The predicted evolution histories of a satellite in the plane of its effective mass $\mu(t)$ versus characteristic orbital size $S(t) \equiv j(t)/200\,\mathrm{km\,s^{-1}}$. The hatched horn-like areas show models with moderate potential growth ($p = 1/3$, upper horn) with a mass loss between exponential ($n = \infty$, upper dashed boundary) and linear ($n = 1$, lower solid boundary), and models with static potential($p = 0$, lower horn) with a mass loss between linear ($n = 1$, upper dashed boundary) and accelerated ($n = 0.3$, lower solid boundary). A massive satellite starts at $t_\mathrm{i} = 4$ Gyr from the upper right corner with an effective mass $\mu(t_\mathrm{i}) = \langle\beta\rangle_\mathrm{i} m_\mathrm{i} = 10^{10}$ M$_\odot$ with angular momentum $j_\mathrm{i} = 250$ km s^{-1} $\times$ 50 kpc, and ends with an effective mass of 10^7 M$_\odot$. For different assumptions of the mass-loss rate, the intermediate mass and position of the remnant are indicated with a time-step of 1 Gyr. Note the failure to deliver remnants to the lower left corner. Also indicated are the estimated orbital size and the mass of the satellite galaxies of the Milky Way and M31.

4.1 Inferring satellite rotation curves and comparing with observations

Indeed we can infer the internal mass distribution, or internal circular velocity curve, of the satellite using the tidal radius criteria. More specifically, the internal circular motion v_cir at the tidal radius $r_\mathrm{t}(t)$ should be in resonance with the orbital frequency of the satellite at the pericentre $r_\mathrm{p}(t)$, meaning that their angular frequencies or time-scales are equal with

$$\frac{r_\mathrm{t}}{v_\mathrm{cir}} = t_\mathrm{cr} = \frac{r_\mathrm{p}}{V_\mathrm{cir}}, \tag{23}$$

where t_cr is the crossing time, and the radii

$$r_\mathrm{t}(t) = \frac{Gm(t)}{v_\mathrm{cir}^2}, \qquad r_\mathrm{p}(t) = \frac{j(t)}{u_\mathrm{p} V_\mathrm{cir}}, \tag{24}$$

where the factor u_p is the boosting factor of the pericentre velocity due to eccentricity. If we define ρ_t as the overall mean density of the satellite at tidal radius r_t, and ρ_amb and $m(t)$ as the average ambient density and the total mass inside the pericentre r_p, then

$$m(t) = \frac{4\pi\rho_\mathrm{t} r_\mathrm{t}^3}{3}, \qquad M(t) = \frac{4\pi\rho_\mathrm{amb} r_\mathrm{p}^3}{3} = \frac{V_\mathrm{cir}^2 r_\mathrm{p}}{G}. \tag{25}$$

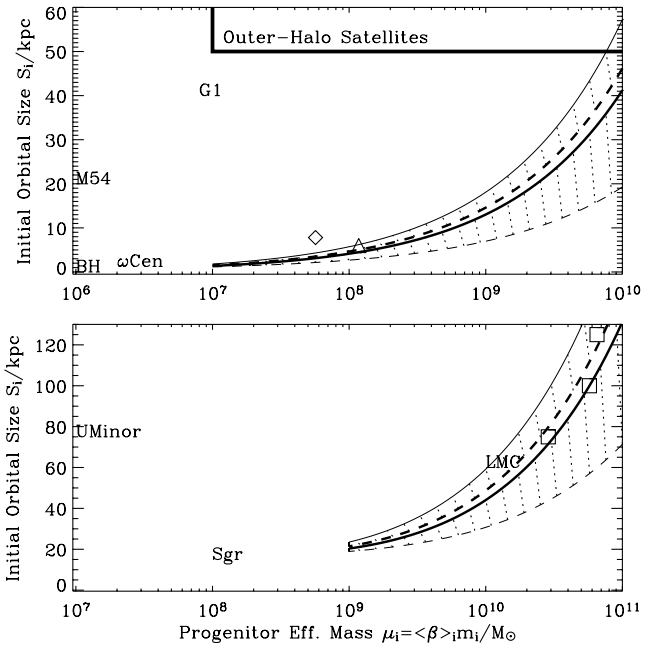

Figure 3. Initial conditions to deliver an ω Centauri-like 10^6-$M_\odot$ remnant to the Galactic Centre (upper panel) or to deliver a Sgr-like remnant of 10^8 $M_\odot$ to the inner Galaxy (lower panel). Dynamical friction works too slowly for an object initially to the upper left of the shaded regions in the plane of the initial effective mass of the progenitor μ_i versus the initial orbital size $S_i = j_i/200$. Different line types and shaded regions have the same meaning as in Fig. 2 (the thick dashed line is for a linear mass loss in a static potential). The symbols are simulations of Bekki & Freeman (diamond) and Tsuchiya et al. (triangle) for ω Centauri, and Jiang & Binney (squares for their models A, F and K) for Sgr; we assume the same Colomb logarithm $\ln\Lambda = 2.5$ for both our model and these simulations. Also indicated are the present values for the several satellites of the Milky Way and M31 and a central million solar mass black hole.

Eliminating r_p and r_t with substitutions, we can rewrite the tidal criteria (equation 23) as follows:

$$\left[\frac{4\pi G\rho_t(t)}{3}\right]^{-1/2} = t_{cr} = \left[\frac{4\pi G\rho_{amb}(t)}{3}\right]^{-1/2}. \quad (26)$$

This means that, as time progresses, the satellite mass $m(t)$ decreases (equation 8), its orbital pericentre $r_p(t)$ decreases (equations 14 and 24), and its mean density $\rho_t(t)$ increases with the ambient density ρ_{amb} (equation 26), hence the tidal radius $r_t(t)$ shrinks with the satellite mass $m(t)$, like what happens with peeling an onion. The tidal peeling-off process effectively maps out ρ_t as a function of m implicitly through these equations. The function $\rho_t(m)$ can then be converted to the internal mass radial profile of the satellite since $r_t(m) \propto [m/\rho_t(m)]^{1/3}$. The circular velocity as a function of enclosed mass m can then be calculated with $v_{cir}^2(m) = Gm/r_t(m)$.

The relation between v_{cir} and the mass $m(t)$ can also be shown more explicitly as follows. From the tidal criteria (equation 23) we have

$$j(t) \propto r_p(t)V_{cir} \propto V_{cir}^2 v_{cir}^{-1} r_t \propto V_{cir}^2 v_{cir}^{-3} m(t) \quad (27)$$

since the tidal radius $r_t = Gmv_{cir}^{-2}$ (cf. equation 24). Substituting in the orbital evolution equation (equation 6), and assuming $\mu(t) \propto m(t)$, we have

$$\frac{d}{dt}\left(mV_{cir}^2 v_{cir}^{-3}\right) \propto \frac{dj(t)}{dt} \propto \frac{m(t)V_{cir}}{j(t)} \propto V_{cir}^{-1} v_{cir}^3. \quad (28)$$

So there is a one-to-one relation between the mass-loss history $m(t)$ and the circular velocity at the tidal radius v_{cir} if we fix the host potential (V_{cir} = constant). Interestingly, this explains why a satellite with flat rotation v_{cir} = constant leads to a linear mass-loss history $(d/dt)m(t)$ = constant.

A few circular velocity curves are shown in Figs 4 and 5. First we consider a hypothetical globular cluster of 10^6 $M_\odot$ on an orbit of apocentre-to-pericentre ratio 15:3 (kpc), which is within the inner galaxy although a slightly bigger orbit than that of ω Centauri. If this cluster is the end result of, say, losing mass linearly with time from a 10^{10}-$M_\odot$ progenitor a Hubble time ago, then the tidal criteria implies a mass profile of the progenitor, shown by the circular velocity curve (labelled $n = 1$) in Fig. 4(b). The progenitor must have a velocity curve close to that of an isothermal cored halo with a tidal radius $r_t \sim 6.5$ kpc. This implies an initial pericentre of about $r_p(t_i) = (200\ \mathrm{km\ s^{-1}}/80\ \mathrm{km\ s^{-1}})r_t \sim 16$ kpc (cf. equation 23). So the progenitor must start out on a small orbit with the first pericentre almost touching the inner halo of the host. Such an orbit is a much smaller than the one that the LMC and Small Magellanic Cloud (SMC) are/were on, which has a pericentre of about 40 kpc now and perhaps even further a Hubble time ago. This result holds qualitatively for a wide range of assumed mass-loss history. When we decrease n from 30 to 0.3, the inferred initial tidal radius increases from $r_t = 4$ to 7.5 kpc (cf. Fig. 4b), corresponding to a pericentre changing from $r_p = 8$ to 20 kpc. The LMC has a tidal radius of about 8–10 kpc. So in order to deliver a final remnant to the inner 15 kpc, we must start with a much smaller orbit and a much denser satellite than the LMC.

It is also remarkable that our predicted circular velocity curves resemble very well those of observed dwarf galaxies, for a variety of initial and final parameters of the satellite and the host galaxy. Rotation curves are shown in Fig. 4(a) for several nearby dwarf galaxies of virial mass $\sim 10^{10}$ $M_\odot$: DDO 154 (Carignan & Purton 1998), NGC 3109 (Jobin & Carignan 1990), NGC 5585 (Blais-Ouellette et al. 1999) and NGC 2976 (Simon et al. 2003). Also indicated (by the locations of the small open circles) are the core radius versus the maximum rotation velocity for a sample of about 50 dwarf galaxies compiled by Sellwood (2000); only those with total mass less than 10^{10} $M_\odot$ are shown here.

The fact that our models give reasonable mass profiles of satellites justifies our empirical parametrization of the mass-loss history (equation 14), and gives a *physical meaning to our n parameter*: $n = 1$ resembles a cored isothermal model, $n \gg 1$ gives an overall solid-body circular velocity curve, and $n \ll 1$ gives a Keplerian-like curve with a dense solid-body core.

Observed dwarf galaxies typically have a solid-body core instead of a cold dark matter cusp, with the density bounded typically between 0.25 and 0.0025 $M_\odot$ pc^{-3}; note that the densest known dwarf galaxy Draco has a core density of 0.7 $M_\odot$ pc^{-3} (Sellwood 2000). These cores imply destruction of typical dwarf galaxies once they decay to pericentres $r_p = 3$–30kpc from a Milky Way host. Among the observed dwarf galaxies, those with a core density comparable to or lower than 0.01 $M_\odot$ pc^{-3} (e.g. DDO 154, NGC 3109) would be torn into tidal streams before sinking into 15 kpc radius of the galaxy.

Similar calculations have also been done for a Sgr-like remnant of 10^8 $M_\odot$ on an orbit of 40 kpc:8 kpc (Fig. 5b). The results for the progenitor are shown and compared with the observed dwarfs on a log–log plot (Fig. 5a). Again the progenitors resemble the observed dwarfs, but again the progenitor must originate from a small orbit.

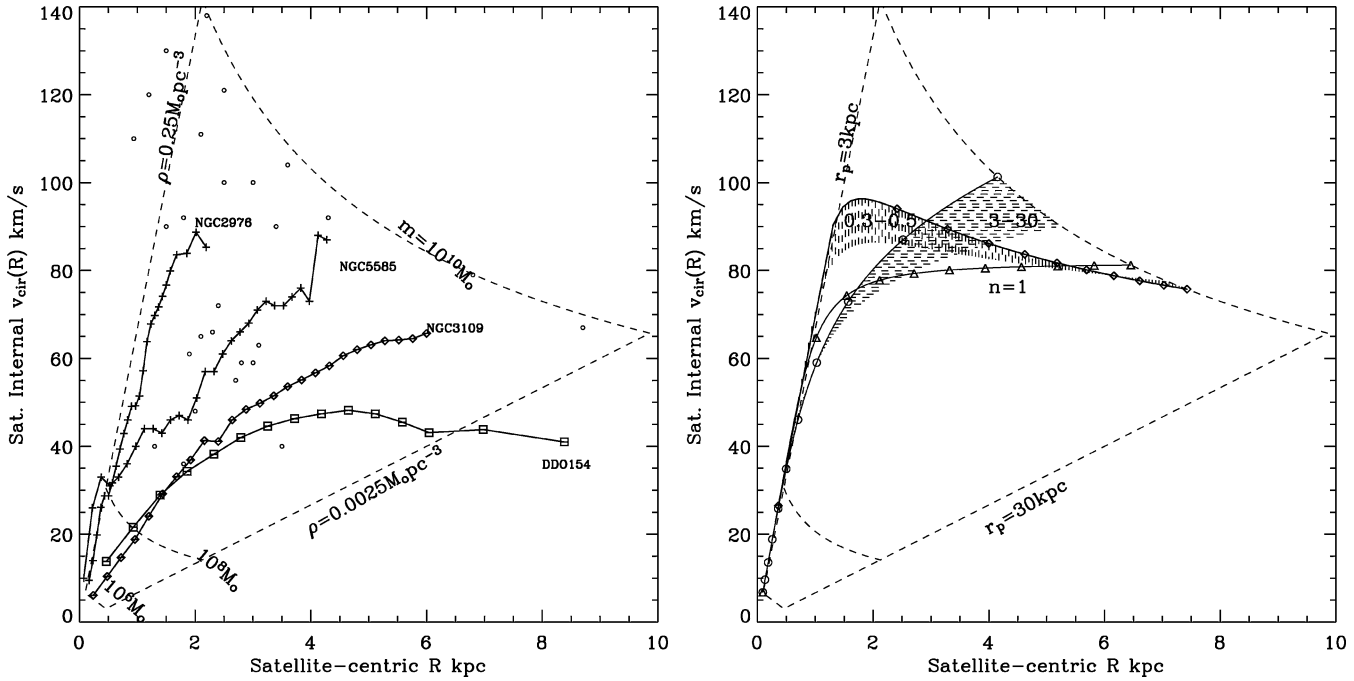

Figure 4. Panel (a) (left) shows the rotation curves of four observed dwarf galaxies (as labelled), and the core radius versus maximum rotation velocity for another two dozen dwarf galaxies (small circles). Also shown is a region bounded by solid-body rotation curves of a uniform volume density $\rho_t = 0.25$ M$_\odot$ or 0.0025 M$_\odot$ pc^{-3} (two thin dashed lines from left to right), and Keplerian rotation curves of a point mass of 10^{10}, 10^8 or 10^6 M$_\odot$ (three thin dashed curves from top to bottom). Panel (b) (right) shows the inferred circular velocity curves of a 10^{10}-M$_\odot$ progenitor for different assumed mass-loss index n; so that a remnant of 10^6 M$_\odot$ is placed on an orbit with an apocentre-to-pericentre ratio of about 15:3 kpc. Symbols indicate the tidal radii at look-back time 1, 2, . . . , 10 Gyr for the $n = 0.3$ model (diamonds), $n = 1$ model (triangles) and $n = 30$ model (circles). Hatched regions are for $n = 0.3$–0.5 and $n = 3$–30.

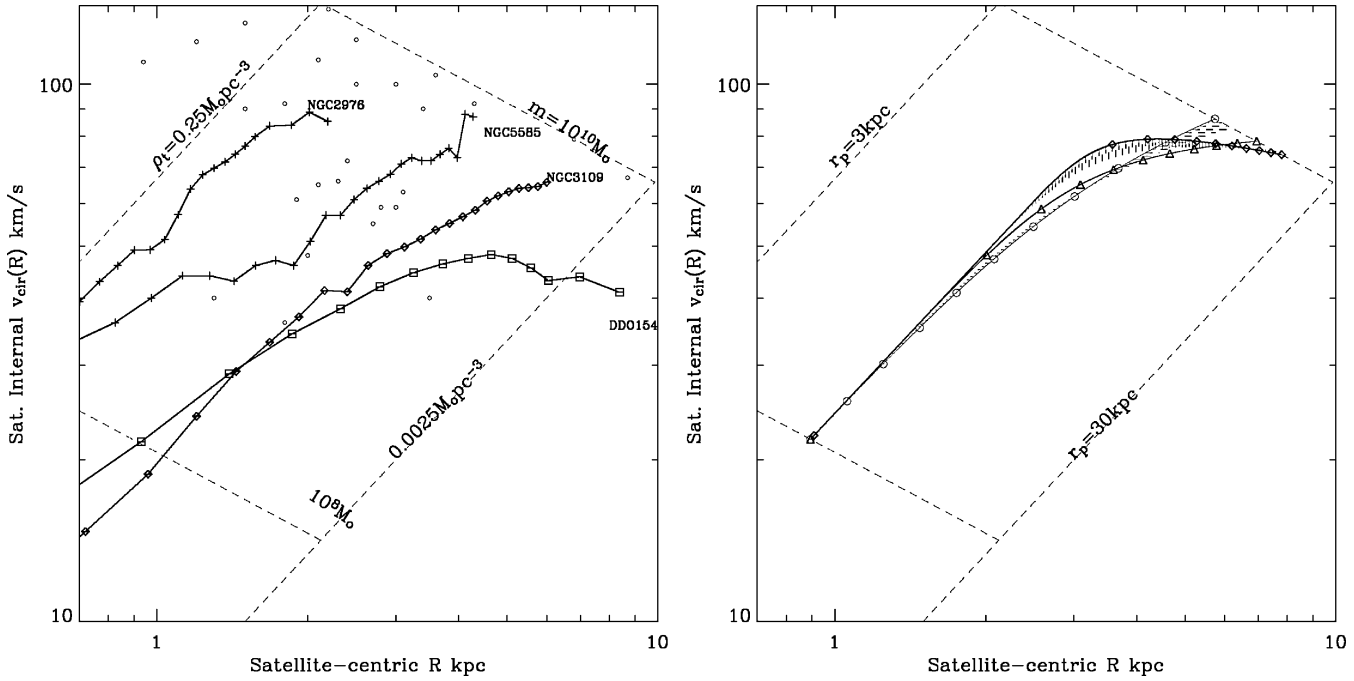

Figure 5. Similar to Fig. 4, except on a logarithmic scale, and for (b) we assume that the remnant is 10^8 M$_\odot$ on an orbit with r_a:r_p = 40 kpc:8 kpc.

4.2 Comparing the analytical model with 'tidal peeling' simulations

A key assumption of our model is that the effective mass is some simple empirical function of time (cf. equation 14) with the normalization $\langle\beta\rangle$ determined by the apo-to-perigalactic ratio (cf. equation 21). In reality the satellite mass is determined by the tides at the pericentre, and the dynamical friction force modulates periodically between pericentre and apocentre. However, these short-time-scale variations are smoothed out when averaged over a Hubble time

and almost do not contribute to the evolution of the orbital angular momentum.

To verify consistency of our empirical mass-loss history (equation 14) with the tidal mass-loss history, we recompute the orbital decay using traditional tidal conditions, similar to Jiang & Binney (2000) and Zhao (2002). Here we fix $\ln\ \Lambda = 2.5$ and show only two general cases with a satellite with an LMC-like flat rotation curve of amplitude $v_{\rm cir} = 70$ km s^{-1} in a host halo of flat circular velocity curve of amplitude $V_{\rm cir} = 200\ (t/14)^{1/9}$ km s^{-1} (i.e. $p = 1/9$). The satellite is launched on an eccentric orbit with the initial specific angular momentum and apocentre-to-pericentre ratio being $j_{\rm i} = 45$ kpc $\times$ 280 km s^{-1} and $C = 3$ for model A, and $j_{\rm i} = 20$ kpc $\times$ 350 km s^{-1} and $C = 8$ for model B, starting from the pericentre (at $r_{\rm p} = 45$ or 20 kpc); the pericentre radius and speed are determined by C according to equation (20), which then determines the initial tidal radius of the satellite (cf. equation 23), and the mass (cf. equation 24). The tidal criteria at the pericentres determine the evolution of the total mass of the satellite (cf. equation 28), which should be slightly non-linear partly due to $V_{\rm cir} \propto t^{1/9}$ and partly due to circularization of the orbit. The satellite orbit is followed for 10 Gyr and shown in Fig. 6. The orbit shrinks and becomes more circular than initially because of dynamical friction, and the satellite loses most of its initial mass. In model A it shrinks from 120/45 kpc to 15/10 kpc, and the mass is reduced by a factor of about 5. In model B it shrinks from the initial apocentre/pericentre of 140/20 kpc to the final one of about 55/15 kpc and the mass is reduced by a factor of about 2.

This is compared with our analytical model for the mass and angular momentum. The initial and final masses of the satellites $m_{\rm i}$ and m_0 are taken from the above tidal-peeling simulations, and also for the the initial and final apocentre-to-pericentre ratios C, which we convert to the initial and final values for $\langle\beta\rangle(C)$ with the help of equation (21) or Fig. 1(b); generally $\langle\beta\rangle_{\rm i} \leqslant \langle\beta\rangle_0$ because of circularization; together these specify the initial and final effective masses $\mu(t_{\rm i})$ and $\mu(t_0)$. We then adopt a simple linear mass-loss $n = 1$ law connecting the the initial and the final (effective) masses of the satellite. The tidal criterion (equation 28) suggest that such a linear mass-loss model would be rigorous for a circular orbit in a static potential ($p = 0$) since the satellite and the galaxy both have flat rotation curves. We then substitute this mass-loss history into equation (8) to predict the past angular momentum $j(t)$ from the present (smaller) value $j(t_0) = j_0$ backwards.[5] The agreement of predictions from the two methods is clearly good overall (cf. Fig. 6b). The agreement is poorer for higher eccentricity orbits with a stronger evolution in eccentricity. This is because our analytical method does not attempt to model the orbital circularization in any detail apart from varying $\langle\beta\rangle$.

We also check our models against previous fully self-consistent live-halo simulations, i.e. simulations using live particles to represent the halo of our Galaxy. We convert the initial conditions of these simulations to calculate $S_{\rm i}$ and $\mu_{\rm i}$. This is shown in Fig. 3. The three simulations (models A, F and K) of Jiang & Binney (2000) require a very massive (10^{10-11} M$_\odot$) progenitor of the Sgr far away (150–250 kpc) from our Galaxy with an initial angular momentum consistent with our linear mass-loss model ($n = 1$, heavy dashed lines in Fig. 3). Here we adopt initial apocentre-to-pericentre ratio $C \sim 200$ kpc/60 kpc and $\langle\beta\rangle_{\rm i} = 0.6$ from their simulations. Jiang & Binney (2000) have also done semi-analytical modelling of orbital decay, and they find that models with $\ln\Lambda = 8.5$ fit best. The discrepancy with our preferred value for $\ln\Lambda \sim 2.5$ is probably due to differences in details of the analytical modelling: their Milky Way halo model has an exponential truncation beyond 200 kpc, which reduces the density and dynamical friction of the halo at 150–250 kpc by about one e-folding. Their definition of the tidal radius also implies a systematically stronger (up to a factor of 2 for model A initially) tide, hence a somewhat smaller satellite. Also their semi-analytical satellites lose mass somewhat more quickly than linearly.

A rough agreement is also seen with self-consistent simulations of ω Centauri, where we adopt $C = 60$ kpc/1 kpc, hence $\langle\beta\rangle_{\rm i} = 0.015$ for the best-fitting H4 model by Tsuchiya et al. (2003), and $C = 26$ kpc/6 kpc, hence $\langle\beta\rangle_{\rm i} = 0.45$ for Bekki & Freeman (2003). There is some discrepancy with Bekki & Freeman, perhaps due in part to our neglecting effects of the disc. The final phase of their merger model is perhaps too violent for Chandrasekhar's analytical description anyway. Indeed their orbit did not circularize – instead the apocentre-to-pericentre ratio increased to 8 kpc:1 kpc, somewhat larger than the observed orbit of ω Centauri. Correcting down their orbital size would make better agreement with our prediction.

5 DISCUSSION

5.1 Effects of disc, bulge and orbital inclination

One limitation of the current analysis is that we assume an isothermal dark matter plus stars model throughout the galaxy, hence the dynamical friction effects of the disc and bulge are not modelled accurately. However, the disc and bulge are not important for our conclusions because we predict mainly the orbital decay in the outer halo where $j > j_{\rm disc} = 3000$ kpc km s^{-1}. Inside 15 kpc, our estimation of dynamical friction by an SIS model is inaccurate only for satellites on low-inclination orbits. If satellites come at random inclinations, it is more common to find high-inclination orbits, for which our models should be fairly accurate even inside 15 kpc.

5.2 Effects of escaping stars

In the part of our formulation where we derive the satellite mass profile, we assume a simplifying static picture that the satellite mass is peeled off in successive layers at the shrinking tidal radius. The picture in N-body simulations is more complicated, since satellite particles at all radii, e.g. the centre of the satellite, could in principle be escaping at any time. So equation (26) sets only a lower limit on the initial density of the satellite. A more rigorous model should make this correction, e.g. by introducing an empirical factor to correct this as in Jiang & Binney (2000).

5.3 Possible orbits of progenitors of the Sgr stream

The Sgr dwarf and the Canis Major dwarf are the closest known dwarf galaxies, about 15 kpc from the centre of the Milky Way and at the edge of the Milky Way disc. The Canis Major dwarf is on a (direct or retrograde) orbit slightly inclined from the plane of the Milky Way, and the Sgr dwarf is on a nearly polar orbit. Both orbits have a fairly low angular momentum with $S \sim 20$ kpc; the data on Sgr are more complete, and show that it oscillates between 10-kpc pericentre and 50-kpc apocentre. Both contain several globular clusters. It is possible that the two dwarfs are the stripped-down version of a more massive object, which has dynamically decayed from the outer halo.

[5] Predicting $j(t)$ from the initial (bigger) value $j(t_{\rm i})$ forwards would be less stable or accurate once $j(t) \to 0$ because the relative error diverges.

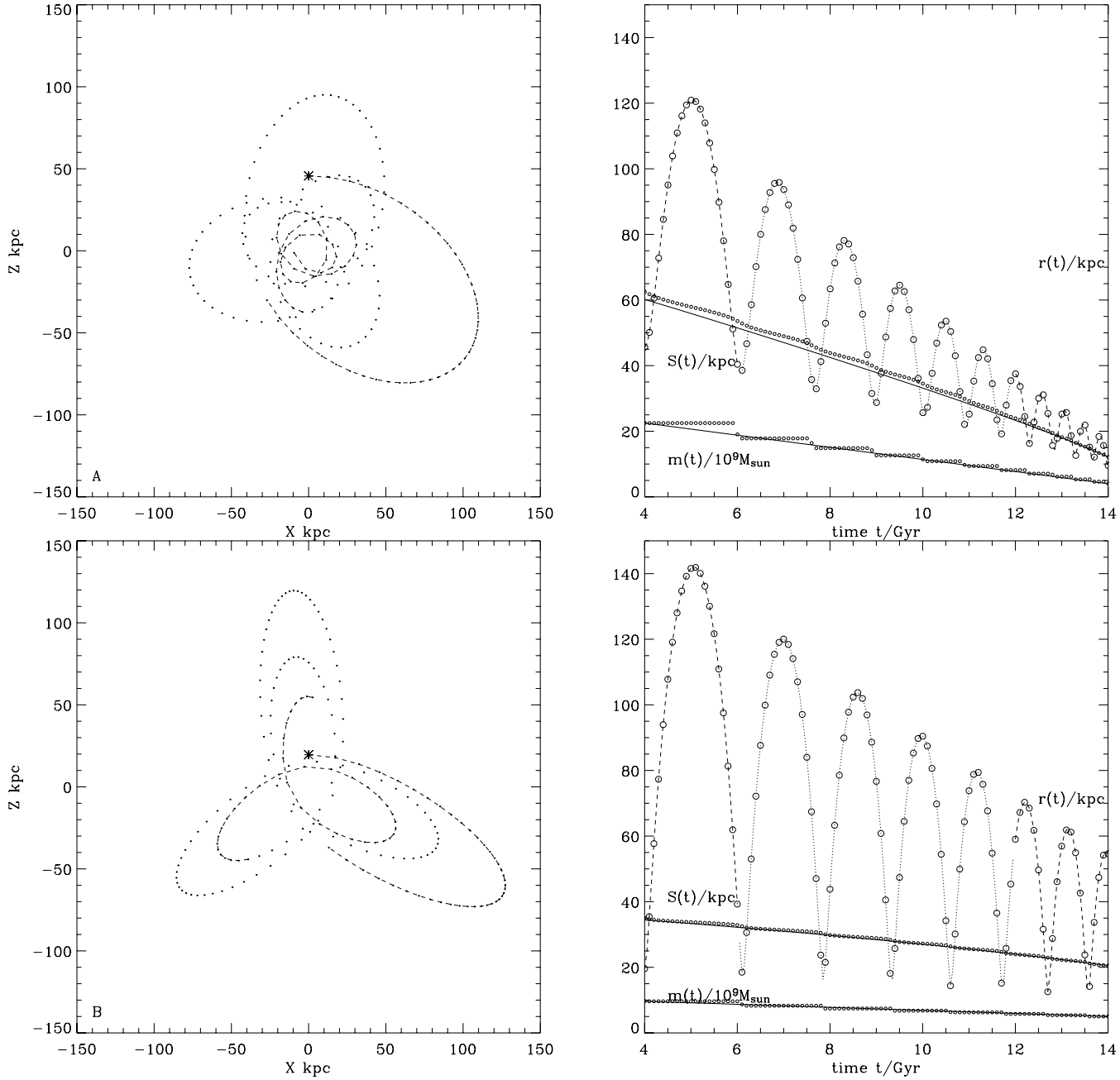

Figure 6. An eccentric satellite orbit launched (from the positions marked by the asterisks) with initial apocentre-to-pericentre ratio $C = 3$ (upper left) and $C = 8$ (lower left, a model for Sgr) in the X–Z plane from $t = 4$–6 Gyr (dashed), $t = 6$–12 Gyr (dotted) and $t = 12$–14 Gyr (dashed). Also shown on the right are the evolution histories of the orbital radius $r(t)$, the orbital size $S(t) = j(t)/200$ km s^{-1} and the mass $m(t)$ by our analytical method (solid line) and the traditional method (points in even time-steps of 0.1 Gyr).

Interestingly, a possible extension of the Sgr dwarf has been reported recently in the Sloan Digital Sky Survey (SDSS) data near the position of the outer halo globular cluster NGC 2419 (Newberg et al. 2003). There is a stream-like enhancement of halo A-coloured stars at the SDSS magnitude of $g_0 = 20.3$ in the plane of the Sgr dwarf orbit, corresponding to a distance of 90 kpc. If this is true, it would imply that the Sgr dwarf has changed its orbits in the past Hubble time. There are two possible ways that this could happen. One is that the orbit of the Sgr dwarf has been deflected by a massive satellite, such as the LMC or SMC. Indeed, the orbits of the Sgr dwarf and the Magellanic Clouds do overlap at the Galactic poles, and simple timing arguments show that these systems encountered or flew by each other about 2.5 Gyr ago at about 50 kpc on the North Galactic Pole if the rotation curve of the Milky Way is nearly flat (Zhao 1998). The problem of this solution is that it is rare for the Sgr dwarf to receive a strong enough deflection to bring down its orbit.

Another solution is that the Sgr dwarf has been a more massive system, the orbit of which decayed from the outer halo (Jiang & Binney 2000). *Our model B illustrates such an example of the progenitor of the Sgr dwarf* which had an initial mass comparable to that of the LMC (10^{10} M$_\odot$) and which was on an eccentric orbit

with radius between 20 and 140 kpc (cf. Fig. 6). This model is similar to model K of Jiang & Binney . After a Hubble time the orbit decays to a small orbit very much like that of the Sgr dwarf with pericentre-to-apocentre ratio of 10 kpc:50 kpc. Large amounts of the material of the progenitor are shed at radii between 10 and 140 kpc; the stream near NGC 2419 at 90 kpc could be part of this debris near one of the apocentres of the orbit. Unfortunately the present model ends with a mass of 5×10^9 $M_\odot$, too large for the present-day Sgr dwarf. Some fine-tuning of initial conditions and detailed *N*-body simulations are clearly needed to test this idea.

5.4 Possible orbits of the progenitor of ω Centauri

We have mainly concentrated on the problem of getting rid of the angular momentum of a satellite if it starts with a high angular momentum or orbital size $S_0 \gg 15$ kpc. What would be the remnant distribution if a satellite were born with an initial orbital size $S_\mathrm{i} < 15$ kpc? The stars in such a system are assembled in the inner halo from the start, e.g. by colliding an infalling gas cloud with the protogalactic gas clouds in the inner halo (Fellhauer & Kroupa 2002). Alternatively, the stars form from extragalactic gas and descend on a very radial orbit, penetrating the inner 15 kpc of the host halo from its very first pericentric passage.

An intriguing example is ω Centauri. Unfortunately, our analytical model is not suited for this system because it is presently on a low-inclination eccentric retrograde orbit between 1 and 6 kpc from the Galactic Centre (Dinescu et al. 1999), so the contribution of dynamical friction by the disc is important. Also hydrodynamical friction with the disc gas can play a role for an early-on partially gaseous satellite. Nevertheless, if one applies simplistically the tidal mass loss and Chandrasekhar's dynamical friction in a spherical halo, one finds that, while it seems easy to peel off a satellite galaxy to make a central star cluster, most simulations produce remnants on much larger orbits than ω Centauri (Zhao 2002). It seems that some fine-tuning is required to select progenitors on very low-angular-momentum and/or low-energy orbits: the initial angular momentum needs to be low enough for the progenitor to penetrate into the inner halo or the present location of ω Centauri on its very first pericentric passage. This means that the initial orbital size S_i^ω of ω Centauri is in between the present value of ω Centauri $S_0 \sim 1.25$ kpc and the boundary of the inner halo $R_\mathrm{disc} = 15$ kpc, or, mathematically,

$$1.25 < S_\mathrm{i}^\omega < 15\mathrm{kpc}. \qquad (29)$$

Most recently there have been several very encouraging attempts to model the dynamical and star formation history of ω Centauri by nearly self-consistent *N*-body simulations (Mizutani, Chiba & Sakamoto 2003; Tsuchiya, Dinescu & Korchagin 2003; Bekki & Freeman 2003). All are able to produce both a reasonable mass and orbit of ω Centauri after some trial and error with the initial parameters of the progenitor; many initial conditions lead to remnants, unlike ω Centauri, beyond 10 kpc of the Milky Way centre. The favoured initial orbit has a small orbital size S_i. According to Tsuchiya et al., $j_\mathrm{i} = 60$ kpc $\times$ 20 km s^{-1} = 1200 kpc km s^{-1} (or $S_\mathrm{i} = 6$ kpc), and according to Bekki & Freeman, $j_\mathrm{i} = 25$ kpc $\times$ 60 km s^{-1} = 1500 kpc km s^{-1} (or $S_\mathrm{i} = 7.5$ kpc). The small orbital size seems consistent with our expectation (cf. Fig. 3).

Tsuchiya et al. launch satellites with various initial masses (0.4–1.6) $\times 10^{10}$ $M_\odot$ and with either a King profile or a Hernquist profile from 60 kpc from the Milky Way centre. They choose well-aimed nearly radial orbits, with an initial perigalactic radius of about 1 kpc, much more radial than the present eccentric orbit. Mass loss in their King model is similar to our exponential mass-loss models ($n = \infty$): rapid at the beginning, and $\log(m)$ is roughly linear with time up to a mass of 10^8 $M_\odot$ when the satellite has too little mass to proceed with the orbital decay. Mass loss in the Hernquist model is closer to a $n = 0.3$ model: linear at the beginning and rapid just before complete disruption (cf. Fig. 1a).

Our comparison with Tsuchiya et al.'s numerical model would be fair apart from one theoretical concern. The progenitor in their best simulation is a two-component 'nucleated' model with a rigid nucleus modelled by a extended particle of 10^7 $M_\odot$ with a half-mass radius of 35 pc on top of a live satellite of 0.8×10^{10} $M_\odot$ with a Hernquist profile of half-mass radius 1.4 kpc; the dynamical friction of the Hernquist halo helps to deliver the nucleus eventually to an orbit similar to that of ω Centauri. However, a closer examination reveals a subtle inconsistency in making the nucleus rigid: the tidal force from the Hernquist halo beats the self-gravity of this fluffy nucleus at its half-mass radius by a factor of a few, so it could not have stayed and been moved as one piece. Nevertheless, one could have used a more compact, and hence a more plausible model of the rigid nucleus, say, with a total mass of 3×10^6 $M_\odot$ and a smaller half-mass radius of 7 pc, which are closer to the observed mass and half-mass radius of ω Centauri. With this in mind, the formal inconsistency in Tsuchiya et al.'s best simulation seems to be harmless, and their model shows that ω Centauri could in principle be the remnant of a massive satellite on an orbit of initial apocentre-to-pericentre ratio of 60 kpc:1 kpc.

6 SUMMARY

We have used a set of simple analytical models of dynamical friction and tidal mass loss to explore the orbital decay for a dwarf satellite with a range of initial specific angular momentum and mass-loss history. These models greatly simplify the orbital dynamics and tidal interaction of satellites without losing the accuracies of more rigorous and sophisticated numerical simulations. We follow the evolution of satellites in the mass–distance plane, and find generally very little evolution of specific angular momentum by dynamical friction. The progenitors of inner halo globular clusters and substructures cannot be born on orbits of comparable angular momentum to present-day halo satellite galaxies. The central cores of observed dwarfs are also not dense enough to survive the tides within 15 kpc. Any black holes in these satellites may also be difficult to reach and merge with the supermassive black hole in the host galaxy. In general, satellite remnants (black holes, globulars and streams) tend to hang up in the outer halo.

ACKNOWLEDGMENTS

I thank Ken Freeman, George Meylan, Jim Pringle and Floor van Leeuwen for enlightening discussions during the ω Centauri conference at IoA, and Oleg Gnedin, Mike Irwin, Pavel Kroupa and Mark Wilkinson for a careful reading of an earlier draft. I thank Vladimir Korchagin, Dana Dinescu and Toshio Tsuchiya for patiently explaining their paper to me, and James Binney and Kenji Bekki for answering queries on their models. This work has been made possible by a special grant of research time from my 1-year-olds MianMian and YiYi.

REFERENCES

Bekki K., Freeman K. C., 2003, MNRAS, 346, L11

Binney J. J., Tremaine S., 1987, Galactic Dynamics. Princeton Univ. Press, Princeton, NJ

Blais-Ouellette S., Carignan C., Amram P., Cŏté S., 1999, AJ, 118, 2123
Carignan C., Purton C., 1998, ApJ, 506, 125
Chandrasekhar S., 1943, ApJ, 97, 255
Dekel A., Devor J., Hetzroni G., 2003, MNRAS, 341, 326
Dinescu D. I., Girard T. M., van Altena W. F., 1999, AJ, 117, 1792
Fellhauer M., Kroupa P., 2002, MNRAS, 330, 642
Ferguson A., Irwin M., Ibata R., Lewis G., Tavir N., 2002, AJ, 124, 1452
Freeman K. C., 1993, in Smith G. H., Brodie J. P., eds, ASP Conf. Ser. Vol. 48, The Globular Cluster–Galaxy Connection. Astron. Soc. Pac., San Francisco, p. 608
Gnedin O. Y., Zhao H., Pringle J. E., Fall S. M., Livio M., Meylan G., 2002, ApJ, 568, L23
Harris W. E., 1996, AJ, 112, 1487
Ibata R. A., Wyse R. F. G., Gilmore G., Irwin M. J., Suntzeff N. B., 1997, AJ, 113, 634
Jiang I., Binney J., 2000, MNRAS, 314, 468
Jobin M., Carignan C., 1990, AJ, 100, 648
Johnston K. V., Zhao H., Spergel D. N., Hernquist L., 1999, ApJ, 512, 109
Kendall P., Magorrian J., Pringle J., 2003, MNRAS, 346, 1078
Klypin A., Zhao H. S., Somerville R., 2002, ApJ, 573, 597
Kroupa P., Bastian U., 1997, New Astron., 2, 77
Larsen S. S., 2001, AJ, 122, 1782
Lynden-Bell D., Lynden-Bell R. M., 1995, MNRAS, 275, 429
McConnachie A. W., Irwin M., Ibata R., Ferguson A., Lewis G., Tavir N., 2003, MNRAS, 343, 1335
McMillan S. L. W., Portegies-Zwart S. F., 2003, ApJ, 596, 314
Martin N. F., Ibata R. A., Bellazzini M., Irwin M. J., Lewis G. F., Dehren W., 2004, MNRAS, 348, 12
Meylan G., Sarajedini A., Jablonka P., Djorgovski S. G., Bridges T., Rich R. M., 2001, AJ, 122, 830
Mizutani A., Chiba M., Sakamoto T., 2003, ApJ, 589, L89
Mouri H., Taniguchi Y., 2003, ApJ, 585, 250
Mulder W. A., 1983, A&A, 117, 9
Newberg H. J. et al., ApJ, 2003, 596, 191
Penarrubia J., Kroupa P., Boily C., 2002, MNRAS, 333, 779
Piatek S. et al., 2002, AJ, 124, 3198
Rich R. M., Mighell K. J., Freedman W. L., Neill J. D., 1996, AJ, 111, 768
Schweizer A. E., Cudworth K., Majewski S., 1997, in Humphreys R. M., ed., ASP Conf. Ser. Vol. 127, Proper Motions and Galactic Astronomy. Astron. Soc. Pac., San Francisco, p. 132
Sellwood J., 2000, ApJ, 540, L1
Simon J. D., Bolatto A. D., Leroy A., Blitz L., 2003, ApJ, 596, 957
Syer D., White S., 1998, MNRAS, 293, 337
Tsuchiya T., Dinescu D. I., Korchagin V. I., 2003, ApJ, 589, L29
van Leeuwen F., Hughes J. D., Piotto G., 2002, eds, ASP Conf. Ser. Vol. 265, Omega Centauri: A Unique Window into Astrophysics. Astron. Soc. Pac., San Francisco, p. 391
Wright L., 2003, PhD thesis, University of Cambridge
Zhao H. S., 1998, ApJ, 500, L149
Zhao H. S., 2002, in van Leeuwen F., Hughes J. D., Piotto G., eds, ASP Conf. Ser. Vol. 265, Omega Centauri: A Unique Window into Astrophysics. Astron. Soc. Pac., San Francisco, p. 391

This paper has been typeset from a TEX/LATEX file prepared by the author.